Methods

A set of speckle-tracking algorithms[5] was used to determine the 1992, 1994, 1995 and 2000 velocities from 1–24-day image pairs. Speckle tracking uses the displacements of the correlated speckle patterns in pairs of SAR images to derive ice motion estimates. Individual errors were up to a few hundred metres per year (see Fig. 2), but errors on averages (for example, Fig. 3) are below 100 m yr^{-1}. We did not tide-correct the speckle-tracked data, so there are biases on the floating ice that do not spatially average out. To assess this error, we estimated velocity for five 1992 InSAR pairs, each with different tidal errors. The standard deviation for these estimates was 69 m yr^{-1}. Our 1992 and 1994 estimates are temporal averages of multiple (2 to 5) same-year pairs, which further reduces this error. The 2001 through 2003 estimates were derived using the IMCORR[25] feature-tracking software applied to 16-to-64-day Landsat image pairs. Established methods[26] were applied to passive microwave data to determine the 2002 melt extent.

Received 7 July; accepted 8 October 2004; doi:10.1038/nature03130.

1. Echelmeyer, K., Clarke, T. S. & Harrison, W. D. Surficial glaciology of Jakobshavns Isbrae, West Greenland. 1. Surface morphology. *J. Glaciol.* **37,** 368–382 (1991).
2. Krabill, W. *et al.* Greenland ice sheet: High-elevation balance and peripheral thinning. *Science* **289,** 428–430 (2000).
3. Thomas, R. H. *et al.* Investigation of surface melting and dynamic thinning on Jakobshavn Isbrae, Greenland. *J. Glaciol.* **49,** 231–239 (2003).
4. Abdalati, W. *et al.* Outlet glacier and margin elevation changes: Near-coastal thinning of the Greenland ice sheet. *J. Geophys. Res.* **106,** 33729–33741 (2001).
5. Joughin, I. Ice-sheet velocity mapping: a combined interferometric and speckle-tracking approach. *Ann. Glaciol.* **34,** 195–201 (2002).
6. Fastook, J. L., Brecher, H. H. & Hughes, T. J. Derived bedrock elevations, strain rates and stresses from measured surface elevations and velocities—Jakobshavns Isbrae, Greenland. *J. Glaciol.* **41,** 161–173 (1995).
7. Abdalati, W. & Krabill, W. B. Calculation of ice velocities in the Jakobshavn Isbrae area using airborne laser altimetry. *Remote Sens. Environ.* **67,** 194–204 (1999).
8. Echelmeyer, K., Harrison, W. D., Clarke, T. S. & Benson, C. Surficial glaciology of Jakobshavns Isbrae, West Greenland. 2. Ablation, accumulation and temperature. *J. Glaciol.* **38,** 169–181 (1992).
9. Zwally, H. J. *et al.* Surface melt-induced acceleration of Greenland ice-sheet flow. *Science* **297,** 218–222 (2002).
10. Echelmeyer, K. & Harrison, W. D. Jakobshavns Isbrae, West Greenland—Seasonal variations in velocity or lack thereof. *J. Glaciol.* **36,** 82–88 (1990).
11. Weidick, A. *Satellite Image Atlas of Glaciers of the World, Greenland* (USGS Professional Paper 1386-C, United States Government Printing Office, Washington, 1995).
12. Sohn, H. G., Jezek, K. C. & van der Veen, C. J. Jakobshavn Glacier, West Greenland: 30 years of spaceborne observations. *Geophys. Res. Lett.* **25,** 2699–2702 (1998).
13. Hughes, T. The Jakobshavns effect. *Geophys. Res. Lett.* **13,** 46–48 (1986).
14. Rott, H., Rack, W., Skvarca, P. & De Angelis, H. Northern Larsen Ice Shelf, Antarctica: further retreat after collapse. *Ann. Glaciol.* **34,** 277–282 (2002).
15. De Angelis, H. & Skvarca, P. Glacier surge after ice shelf collapse. *Science* **299,** 1560–1562 (2003).
16. Scambos, T. A., Hulbe, C., Fahnestock, M. & Bohlander, J. The link between climate warming and break-up of ice shelves in the Antarctic peninsula. *J. Glaciol.* **46,** 516–530 (2000).
17. van der Veen, C. J. Fracture mechanics approach to penetration of surface crevasses on glaciers. *Cold Regions Sci. Technol.* **27,** 31–47 (1998).
18. IPCC. *Climate Change 2001: Working Group I: The Scientific Basis* (eds Houghton, J. T. *et al.*) Ch. 11 ⟨http://www.grida.no/climate/ipcc_tar/wg1/index.htm⟩ (Intergovernmental Panel on Climate Change, Cambridge Univ. Press, Cambridge, 2001).
19. Thomas, R. H. *et al.* Substantial thinning of a major east Greenland outlet glacier. *Geophys. Res. Lett.* **27,** 1291–1294 (2000).
20. Rignot, E., Vaughan, D. G., Schmeltz, M., Dupont, T. & MacAyeal, D. Acceleration of Pine Island and Thwaites glaciers, West Antarctica. *Ann. Glaciol.* **34,** 189–194 (2002).
21. Mohr, J. J., Reeh, N. & Madsen, S. N. Three-dimensional glacial flow and surface elevation measured with radar interferometry. *Nature* **391,** 273–276 (1998).
22. Joughin, I., Tulaczyk, S., Fahnestock, M. & Kwok, R. A mini-surge on the Ryder Glacier, Greenland, observed by satellite radar interferometry. *Science* **274,** 228–230 (1996).
23. Joughin, I., Tulaczyk, S., Bindschadler, R. & Price, S. F. Changes in West Antarctic ice stream velocities: Observation and analysis. *J. Geophys. Res.* **107** (B11), 2289, doi:10.1029/2001JB001029 (2002).
24. Paterson, W. S. B. *The Physics of Glaciers* 3rd edn (Pergamon, Oxford, 1994).
25. Scambos, T. A., Dutkiewicz, M. J., Wilson, J. C. & Bindschadler, R. A. Application of image cross-correlation to the measurement of glacier velocity using satellite image data. *Remote Sens. Environ.* **42,** 177–186 (1992).
26. Abdalati, W. & Steffen, K. Greenland ice sheet melt extent: 1979–1999. *J. Geophys. Res.* **106,** 33983–33988 (2001).

Acknowledgements This work was supported by the Cryospheric Sciences Program of NASA's Earth Science Enterprise. I.J. performed his contribution at the Jet Propulsion Laboratory, California Institute of Technology, under contract with the National Aeronautics and Space Administration. We thank H. Brecher for the 1985 velocity data and B. Csatho, K. In Huh and S. Manizade for acquiring and orthorectifying the Landsat imagery. Radarsat data were provided by CSA through ASF and ERS SAR data were provided by ESA through the VECTRA project.

Author contributions All authors contributed equally to this work.

Competing interests statement The authors declare that they have no competing financial interests.

Correspondence and requests for materials should be addressed to I.J. (ian@apl.washington.edu).

Human contribution to the European heatwave of 2003

Peter A. Stott[1], D. A. Stone[2,3] & M. R. Allen[2]

[1]*Met Office, Hadley Centre for Climate Prediction and Research (Reading Unit), Meteorology Building, University of Reading, Reading RG6 6BB, UK*
[2]*Department of Physics, University of Oxford, Oxford OX1 3PU, UK*
[3]*Department of Zoology, University of Oxford, Oxford OX1 3PS, UK*

The summer of 2003 was probably the hottest in Europe since at latest AD 1500[1–4], and unusually large numbers of heat-related deaths were reported in France, Germany and Italy[5]. It is an ill-posed question whether the 2003 heatwave was caused, in a simple deterministic sense, by a modification of the external influences on climate—for example, increasing concentrations of greenhouse gases in the atmosphere—because almost any such weather event might have occurred by chance in an unmodified climate. However, it is possible to estimate by how much human activities may have increased the risk of the occurrence of such a heatwave[6–8]. Here we use this conceptual framework to estimate the contribution of human-induced increases in atmospheric concentrations of greenhouse gases and other pollutants to the risk of the occurrence of unusually high mean summer temperatures throughout a large region of continental Europe. Using a threshold for mean summer temperature that was exceeded in 2003, but in no other year since the start of the instrumental record in 1851, we estimate it is very likely (confidence level >90%)[9] that human influence has at least doubled the risk of a heatwave exceeding this threshold magnitude.

Temperatures near the Earth's surface are rising globally[10], and evidence is mounting that most of the warming observed in recent decades has been caused by increasing atmospheric concentrations of greenhouse gases[9,11,12]. Anthropogenic increases in annual-mean temperatures have also been detected on continental scales, in Europe, North America and other land regions[13–15]. We first investigate the origins of long-term changes in decadal-mean European summer (June–August) temperatures, determining the changes attributable to anthropogenic drivers of the climate system and changes attributable to natural drivers. We then estimate how the risk of mean June–August temperatures exceeding a particular extreme threshold in any individual summer has changed as a result of this anthropogenic interference in the climate system.

Over the course of the twentieth century, June–August temperatures in Europe exhibited an overall increase, and a distinctive temporal pattern of temperature change, including cooling in the 1950s and 1960s (Fig. 1). We focus on the region bounded by 10° W and 40° E and 30–50° N (Fig. 1 inset), this being one of the regions chosen in previous studies[13,16] to represent climatically coherent regions sufficiently large to exhibit climate change signals above the noise of natural internal variability. We use a pre-selected region in order to minimize any bias that could result from selecting our region already knowing where the most extreme temperatures occurred. Even in such a large domain, 2003 was the warmest summer on record. The history of temperature change averaged over this region is well reproduced by simulations of the HadCM3 climate model[17], even at the model's relatively low spatial resolution (3.75° longitude by 2.5° latitude), when driven with both anthropogenic and natural drivers of climate change (Fig. 1; see red, green, blue and turquoise lines). Four simulations (denoted ALL) were made with different initial conditions[18], each with the same combination of well mixed greenhouse gases, sulphate aerosols and changes in tropospheric and stratospheric ozone, as well as natural changes in solar output and explosive volcanic eruptions[12]. A calculation of the temperature changes due to natural drivers alone (obtained by combining a simulation with solar forcing and

©2004 Nature Publishing Group

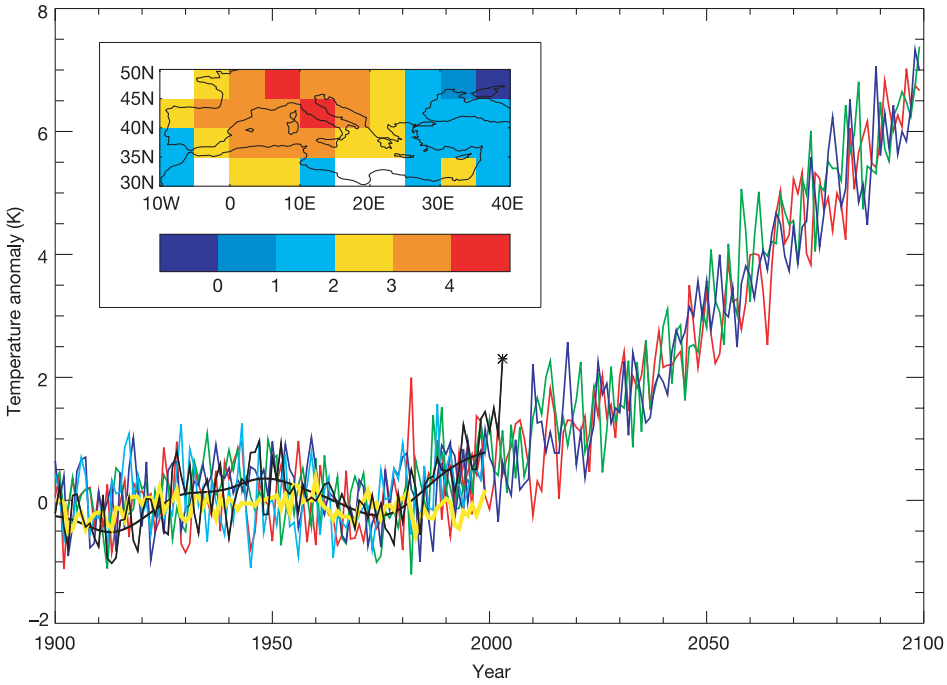

Figure 1 June–August temperature anomalies (relative to 1961–90 mean, in K) over the region shown in inset. Shown are observed temperatures (black line, with low-pass-filtered temperatures as heavy black line), modelled temperatures from four HadCM3 simulations including both anthropogenic and natural forcings to 2000 (red, green, blue and turquoise lines), and estimated HadCM3 response to purely natural natural forcings (yellow line). The observed 2003 temperature is shown as a star. Also shown (red, green and blue lines) are three simulations (initialized in 1989) including changes in greenhouse gas and sulphur emissions according to the SRES A2 scenario to 2100[22]. The inset shows observed summer 2003 temperature anomalies, in K.

a simulation with volcanic forcing, and denoted NAT) shows no warming in the latter part of the century (Fig. 1, yellow line).

A necessary requirement for any detection of significant warming is that HadCM3 adequately represents the natural internal variability of European summer temperatures. A quantitative test, in which an estimate of the forced response calculated from the ALL ensemble mean is subtracted from the observations and the residual compared with HadCM3 simulated internal variability, shows no significant discrepancy in variance on either interdecadal or 2- to 10-year timescales (Fig. 2). If anything, the model appears to be overestimating observed variability in this season and region, making our estimates of attributable risk relatively conservative. We also find no evidence of a secular change in variance on sub-decadal timescales in either model or observations: over the twenty-first century, the standard deviation of the forced simulations under the SRES A2 scenario (Fig. 1), when a second-order polynomial trend has been removed, increases by an insignificant 0.01 K from the first 40 years (1990–2030) to the last 40 years (2060–2100). This contrasts with the conclusions of ref. 2, although their results applied to a much smaller region.

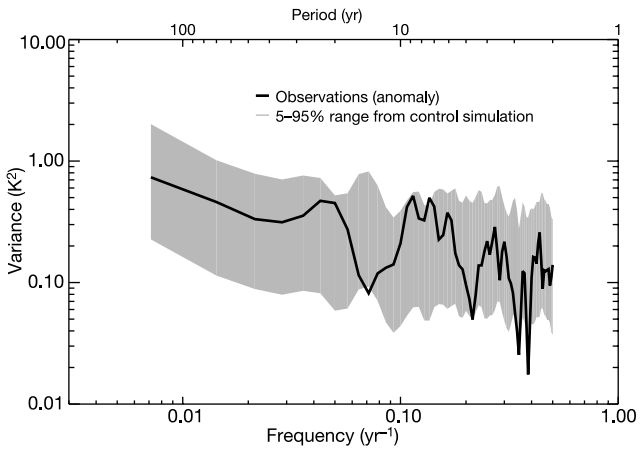

Figure 2 Power spectra of European mean summer temperature. Solid line, observed spectrum after removing an independent estimate of the externally forced response provided by the ensemble mean of the ALL simulations. Shaded region, 5 to 95 percentile region of the estimated range of spectra of natural internal variability estimated from segments taken from the HadCM3 control run of the same length as the observations. Model spectral densities have been inflated by a factor of 1.25 to allow for sampling uncertainty in the ALL ensemble mean.

We now apply a standard optimal detection analysis to European summer temperatures, similar to those applied to global scale patterns of temperature change[11,12,19]. The analysis is a regression between decadal-mean seasonal-mean observations over 1920–99 and simulated temperature changes over the same period from both anthropogenic and natural forcings (ALL) and from natural forcings alone (NAT), and is in most respects identical to that of ref. 13 (see Methods). Figure 3a shows the estimated likelihood functions for the factors by which we could scale up or down the amplitudes of the model-simulated responses to anthropogenic forcing (red curve) and natural forcing (green curve) while remaining consistent with the observations. As the fifth percentile of the scaling factor on the anthropogenic response (red curve in Fig. 3a) is greater than zero, an anthropogenic influence on decadal-mean European summer temperature is detected at the 5% significance level (that is, the hypothesis that there is no positive anthropogenic influence can be rejected at the 5% level). We conclude from this investigation of decadal-mean summer temperatures that it is very likely that past anthropogenic forcing is responsible for a significant fraction of the observed European summer warming.

We now calculate the changed risk of extremely hot summers that can be attributed to past anthropogenic emissions, allowing for

©2004 Nature Publishing Group

uncertainty in the anthropogenic warming. Averaged over the region of interest (Fig. 1 inset), summer temperatures in 2003 exceeded the 1961–90 mean by 2.3 K (Fig. 1, black star). To quantify changes in risk, we need an objective definition of the event in question. Using 2.3 K itself is problematic for three reasons: first, relying too closely on the details of what actually occurred when defining what we are looking for introduces a selection bias in our attribution procedure; second, temperature anomalies in 2003 may have been amplified by soil-moisture feedbacks[2] or interactions with the North Atlantic[20], both of which may be under-estimated, although we do observe similar magnitude spikes in model summer temperatures in Fig. 1; third, given the length of model-simulated variability we have available, inferring the statistics of temperature excursions over 2 K requires extrapolation of extreme value distributions, which introduces further uncertainties. 2003 was the first year to reach or exceed a threshold of 1.6 K (2001 being the second-warmest European summer, at 1.5 K). We therefore consider how the probability of exceeding this threshold has changed, by comparing this estimated late-twentieth-century probability with the estimated probability of exceeding the same absolute threshold if there had been no anthropogenic influence on climate. Increasing this threshold to any value up to 2.3 K strengthens our conclusions regarding attributable risk; hence using a threshold that only just exceeds the second warmest summer is relatively conservative.

Assuming that sub-decadal continental-scale variability is stationary and adequately represented by HadCM3, we estimate possible distributions of temperatures in individual summers in the presence and absence of anthropogenic influence. We do this by adding HadCM3 control variability to reconstructions of 1990s decadal-mean temperatures both with all external factors included, and with anthropogenic factors removed, allowing for uncertainty in these decadal-mean temperatures from the detection analysis (Fig. 3b). Figure 4a shows the estimated likelihood of the risk (probability) of exceeding a 1.6 K threshold in the presence of anthropogenic climate change (red line) and in the absence of anthropogenic change (green line), expressed both as a frequency (number of occurrences per thousand years, bottom axis) and as a return period (top axis). The clear shift from the green to the red distribution implies that an appreciable fraction of the risk of such hot summers can be attributed to human influence on climate. Even in the presence of anthropogenic warming, we conclude that the estimated probability of exceeding 1.6 K appears to be low (best estimate is a 1 in 250 year event (Fig. 4a, red curve) but this risk may be increasing rapidly).

The fraction attributable risk (FAR) is estimated in Fig. 4b (see Methods). In certain circumstances, the figure of relevance in establishing possible liability for compensation has been FAR = 0.5, corresponding to a doubling of risk over natural conditions[21] (meaning that one event in two would have happened naturally). According to our calculation, there is a greater than 90% chance that over half the risk of European summer temperatures exceeding a threshold of 1.6 K is attributable to human influence on climate. Although there is a large spread, reflecting the remaining uncertainties in the effects of climate change on this spatial scale, the anthropogenic FAR could be substantially greater than 0.5. Also marked on Fig. 4b is a vertical line representing an overall 'best estimate' of the human contribution to the increased risk of these very hot European summers[7], given the information that we have available at present. On this basis, human influence is to blame for 75% of the increased risk of such a heatwave.

Our analysis shows that European summers are warming owing to anthropogenic climate change. Under un-mitigated emissions scenarios, summers like 2003 are likely to be experienced more

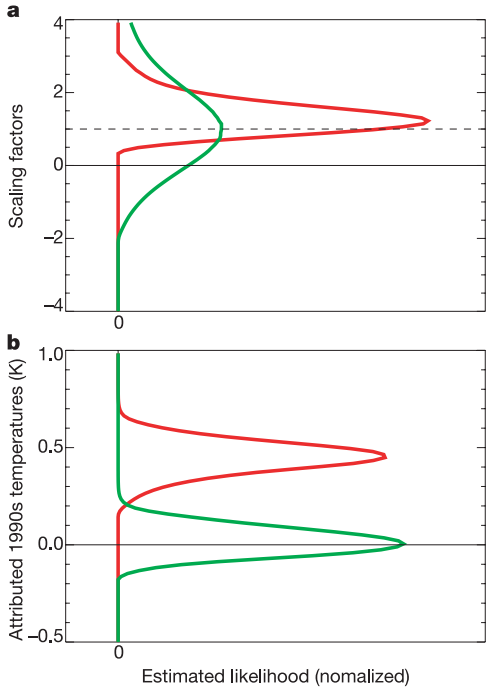

Figure 3 Estimated likelihood functions for anthropogenic and natural contributions to European summer temperature changes. The curves show estimated distributions of anthropogenic (red) and natural (green) scaling factors on model-simulated responses (**a**). 1990s summer temperatures (relative to pre-industrial climate) including all external drivers of climate change (red) and with anthropogenic drivers removed (green) (**b**). A scaling factor of zero (horizontal solid line in **a**) implies no contribution to observed 1990s temperatures from this driver, while unity (horizontal dashed line in **a**) implies no systematic under- or over-estimate by the model of the observed response to this driver. The width of these distributions reflects the uncertainties for these probabilities.

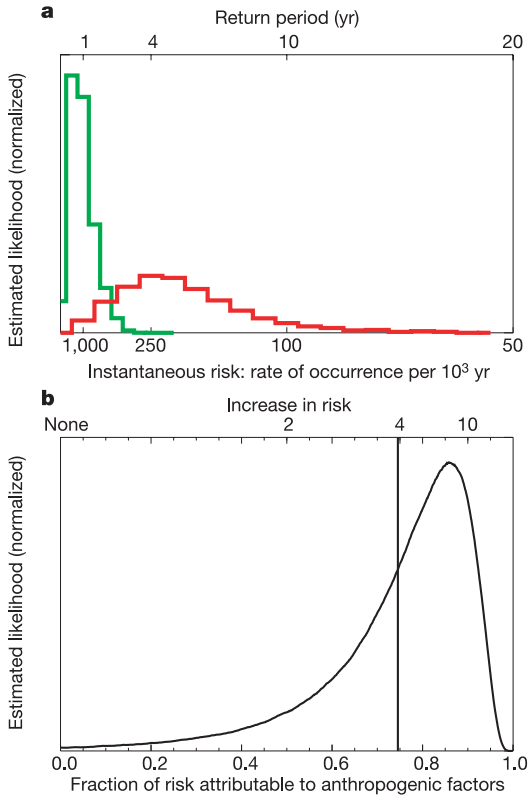

Figure 4 Change in risk of mean European summer temperatures exceeding the 1.6 K threshold. **a**, Histograms of instantaneous return periods under late-twentieth-century conditions in the absence of anthropogenic climate change (green line) and with anthropogenic climate change (red line). **b**, Fraction attributable risk (FAR). Also shown, as the vertical line, is the 'best estimate' FAR, the mean risk attributable to anthropogenic factors averaged over the distribution.

©2004 Nature Publishing Group

frequently in future; HadCM3 projections (Fig. 1) indicate that the probability of European mean summer temperatures exceeding those of 2003 increases rapidly under the SRES A2 scenario[22], with more than half of years warmer than 2003 by the 2040s. By the end of this century, Fig. 1 shows that 2003 would be classed as an anomalously cold summer relative to the new climate, for the scenario and model under consideration.

We may have underestimated the FAR of a heatwave in 2003 by using 1990s figures for attributable background warming. Conversely, the FAR may have been overestimated by selecting an area that has recently been subject to extreme temperatures, although this effect should be alleviated by our use of an independently specified region. Modelling and forcing uncertainties, and any errors in the variability characteristics of the model, could mean that our assessment of the likelihood of the FAR exceeding 0.5 is in error. Including a different combination of the available natural HadCM3 simulations changes the results quoted by less than 5%, but a systematic exploration of both modelling and forcing uncertainty would require a very large multi-model ensemble, varying model parameters across their range of possible values and exploring the range of potential forcing estimates[23,24].

Anthropogenic warming trends in Europe imply an increased probability of very hot summers. Given the effects of the 2003 heatwave, this suggests a greater risk of associated adverse impacts, although to make a quantitative attribution assessment of any specific social, economic or ecological impact will require detailed modelling of both local meteorological conditions and their relationships with the impact in question. Nevertheless, it seems likely that past human influence has more than doubled the risk of European mean summer temperatures as hot as 2003, and with the likelihood of such events projected to increase 100-fold over the next four decades, it is difficult to avoid the conclusion that potentially dangerous anthropogenic interference in the climate system is already underway. The FAR provides a potential measure for redistributing the associated costs of such extreme events[21]. □

Methods

Attribution of decadal-mean seasonal-mean changes

In a natural extension of previous work[12,13,25], observed decadal-mean summer near-surface temperature changes, **y**, over land for 1920–99 are constructed from monthly-mean values extracted from the CRUTEM2(v) data set[10] for the region 10° W-40° E, 30–50° N, requiring data for at least two out of three months (June–August) in at least half the years. They are regressed against the mean response over the observational data-mask of a four-member ensemble of HadCM3 simulations driven with both anthropogenic and natural forcings ($\mathbf{x}_1$, ALL, red, green, blue and turquoise lines in Fig. 1) and a second set of simulations of the response to solar and volcanic forcing alone ($\mathbf{x}_2$, NAT, yellow line in Fig. 1) plus noise:

$$\mathbf{y} = (\mathbf{x}_1 - \nu_1)\beta_1 + (\mathbf{x}_2 - \nu_2)\beta_2 + \nu_0 \quad (1)$$

where β_1, β_2 are the unknown scaling factors to be estimated in the regression, ν_0 is the noise in the observations, and ν_1 and ν_2 account for sampling uncertainty introduced by estimating model-simulated responses from a finite ensemble[26]. A scaling factor of 1 would imply that the response in the model simulations is identical to the observed changes, while a factor of 0 implies no correspondence between modelled and observed responses. Likelihood functions for scaling factors obtained from the regression account only for sampling variability that arises from natural internal climate variability as represented by HadCM3. They do not account for systematic errors in the shapes of the modelled patterns or uncertainties due to missing forcings (for example, land use changes or fossil-fuel black carbon emissions). If we assume a uniform prior in these scaling factors, these likelihoods can be thought of as probability distributions.

The combined effects of solar and volcanic forcings are estimated from a simulation with volcanic forcing amplified by a factor of 10 and solar forcing amplified by a factor of 5, multiplied by 0.1 and 0.2, respectively, and added. This approach was taken in order to obtain the clearest possible climate signal from a weak forcing and a limited number of climate simulations. Previous work showed that the large-scale temperature responds linearly to increasing these forcings[27]. Including an additional four simulations with unamplified natural forcings in the analysis makes little difference to the results.

We use the HadCM3 control run and intra-ensemble variability to estimate internal variability, ν_0, ν_1 and ν_2, taking into account the enhanced signal-to-noise from averaging over the ALL ensemble and inflating the solar and volcanic forcing[13]. This gives scaling factors for the combined effects of all forcings and for natural forcings, from which the anthropogenic and natural scaling factors can be calculated by linear transformation[27] (Fig. 3a). Where the 5 to 95 percentile uncertainty range does not include zero scaling factor, this indicates that the relevant signal has been detected at the 5% significance level, that is, there is less than 5% chance that the relevant forcing has had no effect. From the scaling factors and their uncertainties, we derive likelihood functions of 1990s temperature anomalies attributable to the combined effects of all forcings and attributable to natural factors alone (Fig. 3b).

Attribution of change in risk of exceeding a threshold

The distribution of attributed anthropogenic decadal-mean warming in the 1990s is used to calculate the FAR for an individual European summer exceeding the 1.6 K threshold as follows. We estimate the probability of exceeding the 1.6 K threshold from the generalized Pareto distribution (GPD) fitted to the HadCM3 control run temperatures[28]. The spectral analysis shown in Fig. 2 indicates that HadCM3 provides an adequate representation of internal variability. We calculate the probability, P_0, of the 1.6 K threshold being exceeded without anthropogenic climate change (shown by the green curve in Fig. 4a, expressed as return period, top axis, and instantaneous risk: rate of occurrence per 10^3 yr, bottom axis) and the probability, P_1, of exceeding the threshold with anthropogenic climate change (red curve in Fig. 4a). In estimating the green curve, the chance of exceeding the 1.6 K threshold is re-estimated using the GPD with the mean summer temperature adjusted to each percentile of the estimated distribution of decadal-mean temperature anomalies attributable to natural forcing and internal variability. For the red curve, the response to anthropogenic forcing is also included. A bootstrap resampling method is used to allow for uncertainty in GPD parameters. From these distributions, we calculate the distribution of attributable increase in risk (P_1/P_0) and the FAR ($(P_1 - P_0)/P_1$)[8], as shown in Fig. 4b, whose spread reflects uncertainty in the magnitude of the forced decadal-mean response and in the estimation of the extreme value distribution parameters due to limited sample size.

Received 21 May; accepted 5 October 2004; doi:10.1038/nature03089.

1. Luterbacher, J., Dietrich, D., Xoplaki, E., Grosjean, M. & Wanner, H. European seasonal and annual temperature variability, trends, and extremes since 1500. *Science* **303,** 1499–1503 (2004).
2. Schär, C. *et al.* The role of increasing temperature variability in European summer heatwaves. *Nature* **427,** 332–336 (2004).
3. Beniston, M. The 2003 heat wave in Europe: A shape of things to come? An analysis based on Swiss climatological data and model simulations. *Geophys. Res. Lett.* **31,** doi: 10.1029/2003GL018857 (2004).
4. Black, E., Blackburn, M., Harrison, G. & Methven, J. Factors contributing to the summer 2003 European heatwave. *Weather* **59,** 217–223 (2004).
5. Institut de Veille Sanitaire. Impact sanitaire de la vague chalaire d'aout 2003 en France. Bilan et perspectives. ⟨http://www.invs.sante.fr/publications/2003/bilan-chaleur-1103⟩ (2003).
6. Palmer, T. N. & Räisänen, J. Quantifying the risk of extreme seasonal precipitation events in a changing climate. *Nature* **415,** 512–514 (2002).
7. Allen, M. R. Liability for climate change. *Nature* **421,** 891–892 (2003).
8. Stone, D. A. & Allen, M. R. The end-to-end attribution problem: From emissions to impacts. *Clim. Change* (in the press).
9. IPCC *Climate Change 2001: The Scientific Basis: Contribution of Working Group I to the Third Assessment Report of the Intergovernmental Panel on Climate Change* (eds Houghton, J. T. *et al.*) (Cambridge Univ. Press, Cambridge, UK, 2001).
10. Jones, P. D. & Moberg, A. Hemispheric and large-scale surface air temperature variations: An extensive revision and an update to 2001. *J. Clim.* **16,** 206–223 (2003).
11. Stott, P. A. *et al.* Attribution of twentieth century temperature change to natural and anthropogenic causes. *Clim. Dyn.* **17,** 1–21 (2001).
12. Tett, S. F. B. *et al.* Estimation of natural and anthropogenic contributions to 20th century temperature change. *J. Geophys. Res.* **107,** doi: 10.1029/2000JD000028 (2002).
13. Stott, P. A. Attribution of regional-scale temperature changes to anthropogenic and natural causes. *Geophys. Res. Lett.* **30,** doi: 10.1029/2003GL017324 (2003).
14. Karoly, D. J. *et al.* Detection of a human influence on North American climate. *Science* **302,** 1200–1203 (2003).
15. Zwiers, F. W. & Zhang, X. Towards regional scale climate change detection. *J. Clim.* **16,** 793–797 (2003).
16. Giorgi, F. Variability and trends of sub-continental scale surface climate in the 20th century. Part I: observations. *Clim. Dyn.* **18,** 675–691 (2002).
17. Johns, T. C. *et al.* Anthropogenic climate change for 1860 to 2100 simulated with the HadCM3 model under updated emissions scenarios. *Clim. Dyn.* **20,** 583–612 (2003).
18. Stott, P. A. *et al.* External control of 20th century temperature by natural and anthropogenic forcings. *Science* **290,** 2133–2137 (2000).
19. Tett, S. F. B., Stott, P. A., Allen, M. R., Ingram, W. J. & Mitchell, J. F. B. Causes of twentieth century temperature change near the Earth's surface. *Nature* **399,** 569–572 (1999).
20. Colman, A. & Davey, M. Prediction of summer temperature, rainfall and pressure in Europe from preceding winter North Atlantic ocean temperature. *Int. J. Climatol.* **19,** 513–536 (1999).
21. Grossman, D. A. Warming up to a not-so-radical idea: Tort-based climate change litigation. *Colombia J. Environ. Law* **28,** 1–61 (2003).
22. Nakicenovic, N. & Swart, R. *Special Report on Emission Scenarios* (Cambridge Univ. Press, Cambridge, UK, 2000).
23. Allen, M. R. & Stainforth, D. A. Towards objective probabilistic climate forecasting. *Nature* **419,** 228 (2002).
24. Murphy, J. M. *et al.* Quantification of modelling uncertainties in a large ensemble of climate change simulations. *Nature* **430,** 768–772 (2004).
25. Allen, M. R. & Tett, S. F. B. Checking for model consistency in optimal fingerprinting. *Clim. Dyn.* **15,** 419–434 (1999).
26. Allen, M. R. & Stott, P. A. Estimating signal amplitudes in optimal fingerprinting, Part I: theory. *Clim. Dyn.* **21,** 477–491 (2003).
27. Stott, P. A., Jones, G. S. & Mitchell, J. F. B. Do models underestimate the solar contribution to recent climate change? *J. Clim.* **16,** 4079–4093 (2003).
28. Coles, S. *An Introduction to Statistical Modeling of Extreme Values* (Springer, London, 2001).

©2004 Nature Publishing Group

Acknowledgements P.A.S. was supported by the Department for Environment, Food and Rural Affairs, D.A.S. by a Wellcome Trust Showcase Award, and M.R.A. received partial support from the NOAA/DoE International Detection and Attribution Group.

Competing interests statement The authors declare that they have no competing financial interests.

Correspondence and requests for materials should be addressed to P.A.S. (peter.stott@metoffice.gov.uk).

Evidence for cultivar adoption and emerging complexity during the mid-Holocene in the La Plata basin

José Iriarte[1], Irene Holst[1], Oscar Marozzi[2], Claudia Listopad[3], Eduardo Alonso[4], Andrés Rinderknecht[5] & Juan Montaña[6]

[1]*Center for Tropical Paleoecology and Archaeology, Smithsonian Tropical Research Institute, Box 2072, Balboa, Panama*
[2]*Departamento de Antropología, Facultad de Humanidades y Ciencias de la Educación, Magallanes 1577, Montevideo 1200, Uruguay*
[3]*Florida Institute of Technology, Department of Biological Sciences, 150 West University Boulevard, Melbourne, Florida 32901-6975, USA*
[4]*Departamento de Botánica, Facultad de Química, Universidad de la República, Avda. Gral. Flores 2124, Montevideo, Uruguay*
[5]*Museos Nacionales de Historia Natural y Antropología, Casilla de Correo 339, Montevideo, Uruguay*
[6]*Facultad de Agronomía, Universidad de la República, Av. Garzón 780, Montevideo 12900, Uruguay*

Multidisciplinary investigations at the Los Ajos archaeological mound complex in the wetlands of southeastern Uruguay challenge the traditional view that the La Plata basin was inhabited by simple groups of hunters and gatherers for much of the pre-Hispanic era[1–4]. Here we report new archaeological, palaeoecological and botanical data indicating that during an increasingly drier mid-Holocene, at around 4,190 radiocarbon (^{14}C) years before present (BP), Los Ajos became a permanent circular plaza village, and its inhabitants adopted the earliest cultivars known in southern South America. The architectural plan of Los Ajos during the following Ceramic Mound Period (around 3,000–500 ^{14}C yr BP) is similar to, but earlier than, settlement patterns demonstrated in Amazonia[5–10], revealing a new and independent architectural tradition for South America.

Research on the emergence of complex societies in South America has mainly concentrated on Andean coastal and highland valleys[11–14], and more recently in the lowland forest and riverine regions of Amazonia[5–10]. The La Plata basin (Fig. 1a) is a large and little explored river system that is beginning to reveal an early and long sequence of unique and complex cultural trajectories. The natural environment of the study area is dominated by subtropical grasslands interspersed with vast extensions of wetlands. In strategic locations circumscribed to wetland floodplains, archaeological mound complexes are large and numerous. They have mounded architecture geometrically arranged in circular, elliptical and horseshoe formats that surround a central communal space (Fig. 1b).

The first excavations at the multi-mound site called Los Ajos, by Bracco[15], in the early 1990s consisted of a block excavation in Mound Alfa, a test unit in Mound Beta and a few opportunistic test units in off-mound areas. This work established the mid-Holocene age of the earthen mounds in the area. The Preceramic Mound Period (PMP) component at Los Ajos yielded five dates between 3,950 and 3,350 ^{14}C yr BP (4,580 and 3,380 calibrated (cal.) yr BP)[16]. Closely comparable dates from the deeper PMP components of the Puntas de San Luis, Isla Larga and Potrerillo sites collectively ascertained the antiquity of the PMP[17–19] (Table 1).

Our new excavation programme consisted of the placement of a block excavation in Mound Gamma, a test unit in Mound Delta, two trench transects articulating mound and off-mound areas and a 50-m systematic interval transect sampling strategy of test units to target off-mound areas (Fig. 2) totalling an excavated area of 305 m^2 (ref. 20). Our work revealed that Los Ajos is one of the largest and most formally laid out sites in the study area and covers about 12 ha (Fig. 2a). Its Inner Precinct includes six flat-topped, quadrangular platform mounds (called 6, Alfa, Delta, Gamma, 4 and 7) closely arranged in a horseshoe formation and with a height above ground level of 1.75 to 2.5 m (Fig. 2a, b). Two dome-shaped mounds (called Beta and 8) frame the central, oval plaza with a size of 75 × 50 m (Supplementary Fig. 1a). The formal and compact Inner Precinct contrasts with more dispersed and informally arranged peripheral sectors, which include two crescent-shaped rises (named TBN (Supplementary Fig. 1b) and TBS), five circular and three elongated lower dome-shaped mounds, borrow pits and a vast off-mound area bearing subsurface occupational refuse.

A series of major social and economic changes took place at Los Ajos during the PMP. The broad contemporaneity of radiocarbon dates (Table 1), artefact content and similarities in Preceramic Mound Component (PMC) stratigraphy among mounds Alfa, Delta and Gamma suggest that the Los Ajos inhabitants began to live in a circular household-based community, partitioning the site into a number of discrete functional areas characterized by the placement of residential units around a central plaza area. Charcoal from the basal level of Mound Gamma, 270–275 cm deep (arbitrary depth), dates the beginning of the PMC at 4,190 ± 40 ^{14}C yr BP (4,840–4,580 cal. yr BP). Another radiocarbon assay at 205–210 cm deep yielded a date of around 3,460 ^{14}C yr BP (3,980–3,470 cal. yr BP). The upper portion of the PMC in Mound Delta yielded a date of around 2,960 ± 120 ^{14}C yr BP. Taken together, the eight dates from Los Ajos place the PMC occupation between 4,190 ± 40 and 2,960 ± 40 ^{14}C yr BP. The two oldest dates from the basal levels of the PMC at Mound Gamma and Alfa suggest that mound-building began between around 4,190 and 3,950 ^{14}C yr BP (4,840–4,160 cal. yr BP). Mounds grew as a result of multiple overlapping of domestic occupations where a wide range of activities associated with food preparation, consumption, stone tool production and maintenance took place. The PMC Layer 4 is characterized by a ~85-cm-thick compact, very dark brown silty loam organic sediment (Fig. 3) consisting of relatively undifferentiated deposits composed of lithic debitage and tools, small fragments of charred bone, ash and soot lenses, and small pieces of burned clay.

Our associated palaeoecological data[20] indicate that, similar to other regions in the Americas[21], the mid-Holocene (between 6,620 ± 40 ^{14}C yr BP (7,580–7,440 cal. yr BP) and 4,020 ± 40 ^{14}C yr BP (4,570–4,410 cal. yr BP)) was a period of significant environmental flux marked by increasing aridity. At around 4,020 ^{14}C yr BP (4,570–4,410 cal. yr BP) a maximum drying episode occurred, as evidenced by a massive spike of Amaranthaceae/Chenopodiaceae coupled with a sharp drop in wetland species (Supplementary Fig. 2). These changes probably caused a decrease in the surface water recharge to the inland wetlands and waterways. Although reduced in extent, wetlands probably became attractive places for pre-Hispanic populations by providing abundant, now more highly circumscribed plant and animal resources and a stable source of water. The mid-Holocene drying trend may thus have acted as an important catalyst for the reorientation of settlements towards the topographically higher freshwater wetlands, where permanent communities were established.

Despite the application of an intensive flotation program, seeds, roots and nuts were not recovered; however, phytoliths and starch grains were abundant (Methods are available as Supplementary Information). Phytoliths diagnostic of maize cobs[22] (Fig. 4c) record their earliest appearance in the level from 255–260 cm deep, 15 cm

©2004 Nature Publishing Group

CORRIGENDUM

doi:doi:10.1038/nature04100

Magnetic carbon

Tatiana L. Makarova, Bertil Sundqvist, Roland Höhne, Pablo Esquinazi, Yakov Kopelevich, Peter Scharff, Valerii A. Davydov, Ludmila S. Kashevarova & Aleksandra V. Rakhmanina

Nature **413**, 716–718 (2001)

In this Letter, there was a mistake in the presentation of the synthesis conditions of the reported samples. The actual range of the temperatures of synthesis for the four rhombohedral samples was 975–1,025 K. One of the five reported samples was wrongly characterized in relation to the polymerization type: the sample was actually prepared at 2.5 GPa (synthesis temperature, 1,125 K), representing a mixture of the rhombohedral and tetragonal phases with some hard carbon. The error in characterization of this sample weakens our attribution of the ferromagnetism to defects in the rhombohedral phase (Rh-C_{60}) but does not influence our main conclusion concerning the observation of magnetism in a carbon solid based on polymerized fullerenes, although its origin and the actual magnitude remain an open question. Also, we were unaware of earlier work on magnetism in polymerized fullerenes[1], that should have been cited.

T.L.M. takes full responsibility for the misidentification of the sample preparation conditions. We thank A. V. Talyzin for alerting us to this mistake.

1. Murakami, Y. & Suematsu, H. Magnetism of C_{60} induced by photo-assisted oxidation. *Pure Appl. Chem.* **68**, 1463–1467 (1996).

CORRIGENDUM

doi:10.1038/nature04099

Human contribution to the European heatwave of 2003

P. A. Stott, D. A. Stone & M. R. Allen

Nature **432**, 610–614 (2004)

The description of the method used for the calculation of the fraction attributable risk (FAR) shown in Fig. 4b is incorrect. The corresponding sentence in the Methods section should read "For the red curve, the response to anthropogenic forcing is also included, and a normal distribution is used to estimate the chance of exceeding the 1.6 K threshold."

ERRATUM

doi:10.1038/nature04102

Measurement of the conductance of single conjugated molecules

Tali Dadosh, Yoav Gordin, Roman Krahne, Ilya Khivrich, Diana Mahalu, Veronica Frydman, Joseph Sperling, Amir Yacoby & Israel Bar-Joseph

Nature **436**, 677–680 (2005)

In Fig. 4a of this Letter, in which the spectra of two BPD dimmers are compared, the scaling on the two *y* axes should have been shifted relative to one another in order to illustrate the point made in the text. The corrected Fig. 4a is shown here.

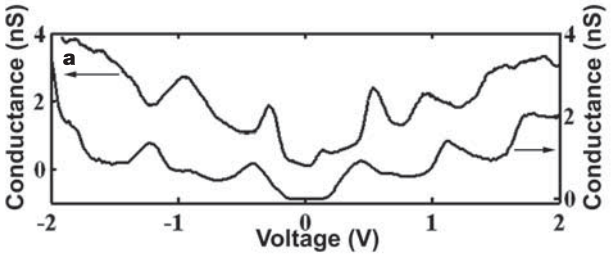

© 2005 Nature Publishing Group